Mon. Not. R. Astron. Soc. **000**, 000–000 (0000) Printed 2 February 2008 (MN LATEX style file v2.2)

Quenching Cluster Cooling Flows with Recurrent Hot Plasma Bubbles

Claudio Dalla Vecchia,[1⋆] Richard G. Bower,[1] Tom Theuns,[1,2] Michael L. Balogh,[1] Pasquale Mazzotta,[3] and Carlos S. Frenk[1]

[1] *Institute for Computational Cosmology, University of Durham, South Road, DH1 3LE Durham, UK*
[2] *University of Antwerp, Campus Drie Eiken, Pleinlaan 1, B-2610 Antwerpen, Belgium*
[3] *Dipartimento di Fisica, Università di Roma "Tor Vergata", via della Ricerca Scientifica 1, I-00133 Roma, Italy*

2 February 2008

ABSTRACT

The observed cooling rate of hot gas in clusters is much lower than that inferred from the gas density profiles. This suggests that the gas is being heated by some source. We use an adaptive-mesh refinement code (FLASH) to simulate the effect of multiple, randomly positioned, injections of thermal energy within 50 kpc of the centre of an initially isothermal cluster with mass $M_{200} = 3 \times 10^{14}$ M$_\odot$ and $kT = 3.1$ keV. We have performed eight simulations with spherical bubbles of energy generated every 10^8 years, over a total of 1.5 Gyr. Each bubble is created by injecting thermal energy steadily for 10^7 years; the total energy of each bubble ranges from 0.1–3$\times 10^{60}$ erg, depending on the simulation. We find that 2×10^{60} erg per bubble (corresponding to a average power of 6.3×10^{44} erg s^{-1}) effectively balances energy loss in the cluster and prevents the accumulation of gas below $kT = 1$ keV from exceeding the observational limits. This injection rate is comparable to the radiated luminosity of the cluster, and the required energy and periodic timescale of events are consistent with observations of bubbles produced by central AGN in clusters. The effectiveness of this process depends primarily on the total amount of injected energy and the initial location of the bubbles, but is relatively insensitive to the exact duty cycle of events.

Key words: galaxies:clusters:general–cooling flows–X-ray:galaxies:clusters

1 INTRODUCTION

Gas cooling at the centre of a cluster halo is an inherently unstable process: cooling increases the gas density, which in turn enhances the cooling rate. X-ray observations show that the cooling time of gas in most cluster cores is less than the Hubble time (e.g. Fabian & Nulsen 1977). Unless cooling is balanced by some form of heating, gas will flow into the cluster centre at rates up to ~ 1000 M$_\odot$yr^{-1} (e.g. Peterson et al. 2001). What happens to the cooled gas is unclear; it could be consumed by star formation, or lead to a reservoir of low temperature (< 1 keV) material in the core. Although this may be the fate of a fraction of the gas, there are indications that most gas in fact does not follow either route. First, the star formation rates in the central galaxies of clusters are much lower than the inferred mass inflow rates (O'Connell & McNamara 1989; Johnstone, Fabian, & Nulsen 1987), rarely approaching ~ 100 M$_\odot$yr^{-1}. To estimate the star formation rate in a typical cluster, we can average over the large sample of clusters studied by Crawford et al. (1999). This suggests that the typical star formation rate is less than 10 M$_\odot$yr^{-1}. Secondly, we can compare the mass deposition rates with observations of the molecular gas content of clusters. Edge (2001) finds molecular gas masses ranging from 10^9 to 2×10^{11} M$_\odot$, with an average of 2.6×10^{10} M$_\odot$. Assuming a gas consumption timescale of 10^9 years (see Edge 2001), this implies a deposition rate that may be as high as 200 M$_\odot$yr^{-1} in a few clusters, but is ~ 30 M$_\odot$yr^{-1} on average. Similar limits are obtained by Salomé & Combes (2003). Finally, recent spectroscopic X-ray observations show no evidence for significant gas cooling below 1 keV (Kaastra et al. 2001; Peterson et al. 2001; Tamura et al. 2001), and observations of molecular and neutral material reveal that the amount of cold gas in clusters of galaxies is also much less than expected from the integrated cooling flow rate (typically less than 30 M$_\odot$yr^{-1} – Edge et al. 2002; Edge & Frayer 2003; Salomé & Combes 2003).

⋆ claudio.dalla-vecchia@durham.ac.uk

This cooling-flow paradox has led many authors to investigate mechanisms to quench gas cooling. Observations of merging clusters show little evidence for cooling flows, which suggests that the merger process might be implicated in disrupting cooling. Recent simulations have shown that sub-halo merging can indeed heat up gas (Burns et al. 2003); however, the amount of cold gas produced in these simulations is still too large compared to that observed, leading to the conclusion that additional heating processes must be involved. Several alternatives have been proposed, including energy injection from radio sources or active galactic nuclei (AGN; Binney & Tabor 1995; Quilis, Bower, & Balogh 2001; Churazov et al. 2002), viscous dissipation of sound waves (Fabian et al. 2003; Ruszkowski, Brüggen, & Begelman 2003) and thermal conduction (Voigt & Fabian 2003; Dolag et al. 2004). Each of these has advantages and disadvantages. In particular, it is difficult to balance cooling, with its ρ^2 density dependence, with heating processes that typically scale as ρ. Since cooling and heating can then balance only at one particular density, some of these feedback mechanisms may lead to unstable solutions with some regions of the cluster being efficiently heated while others continue to cool catastrophically.

AGN are particularly promising candidates for balancing cooling, given their potentially large energy reservoir (Tabor & Binney 1993; Binney & Tabor 1995; Bower et al. 2001). In most numerical simulations of this process to date, energy injection produces bubbles at high temperature and low density that, after a short expansion phase, gain momentum by buoyancy (Brüggen & Kaiser 2001; Quilis, Bower, & Balogh 2001; Basson & Alexander 2003). This mimics the effect of a jet which rapidly loses its collimation, as often observed in local clusters (Eilek 2003). In other simulations, gas is injected at high velocity to mimic jets which retain their large-scale coherence (Reynolds, Heinz, & Begelman 2002; Omma et al. 2003). In this paper, we consider the first mechanism and show that such bursts of localised energy can induce convection of the intra-cluster medium (ICM), which leads to a quasi-stable cluster configuration and reduces the average mass deposition rate to within observational limits. We discuss whether the required energy and duty cycle of AGN activity are compatible with observational limits. This paper is organised as follows. In Section 2 we describe the setup of our simulations and discuss the parameters explored. Results are presented in Section 3 and, in Section 4, we compare the required energy and duty cycle with observational constraints. Finally, our conclusions are summarised in Section 5.

2 SIMULATIONS

In order to concentrate our numerical resolution on the interactions between the cooling material and the buoyant hot bubbles, our simulations use a fixed external gravitational potential and neglect the self-gravity of the gas. This allows us to run the simulation over cosmologically significant timescales. We model the input of energy as a cycle of energy injection and quiescent phases. In the active phase a small region of the gas is heated so that it expands to form a bubble that rises out of the confining potential.

name	E 10^{60} erg	Injected/Radiated Power $\dot{E}_i$ 10^{44} erg s^{-1}	$< \dot{E}_r >_{100}$ 10^{44} erg s^{-1}
A	0	0	no cooling
S0.0	0	0	28
S0.1	0.1	0.32	18
S0.3	0.3	0.95	18
S0.6	0.6	1.9	13
S1.0	1.0	3.2	13
S1.5	1.5	4.7	8.7
S2.0	2.0	6.3	7.9
S3.0	3.0	9.5	6.8

Table 1. Summary of the nine simulations performed. The different simulations are referred to as Sn, where the energy E of a single bubble is $n \times 10^{60}$ erg. $\dot{E}_i$ is the mean energy injection rate over a duty cycle, and $< \dot{E}_r >_{100}$ is the mean emitted energy rate, averaged over the last 10^8 yr of the simulation.

2.1 The code

Our simulations were performed with Flash 2.2, an Adaptive Mesh Refinement (AMR) hydrodynamical code developed and made public by the ASCII Center at the University of Chicago (Fryxell et al. 2000). Flash is a modular block structured AMR code, parallelised using the Message Passing Interface (MPI) library.

Flash solves the Riemann problem on a Cartesian grid using the Piecewise-Parabolic Method (PPM; Woodward & Colella 1984). It uses a criterion based on the dimensionless second derivative $\mathcal{D}^2 \equiv |(Fd^2F/dx^2)/(dF/dx)^2|$ of a fluid variable F to increase the resolution adaptively whenever $\mathcal{D}^2 > c_2$ and de-refine the grid when $\mathcal{D}^2 < c_1$, where $c_{1,2}$ are tolerance parameters. When a region requires refining ($\mathcal{D}^2 > c_2$), child grids with cell size half that of the parent grid are placed over the offending region, and the coarse solution is interpolated. In our simulations, we have used density and temperature as the refinement fluid variable F (see Fryxell et al. 2000, for more details). We have performed a series of simulations with a different maximum level of refinement to investigate the effect of numerical resolution, as described in Section 2.4

Flash interpolates the imposed analytic gravitational potential (see Section 2.2) to the grid cells, and computes the corresponding gravitational acceleration, neglecting the self-gravity of the gas. To interpolate the initial density field from our analytical solution to the Flash mesh, we impose an initial grid with increasing resolution from large radii to the centre of the cluster. This is the minimum refinement level allowed during the simulation.

For the boundary conditions, we impose that the values of density, temperature and velocity on the boundary cells (guard cells) remain the ones computed at the initial time and satisfy the hydrostatic equilibrium conditions. With the cluster located at the centre of the box, the box size of 6×10^{24} cm (1.9 Mpc) is large enough to ensure that cooling

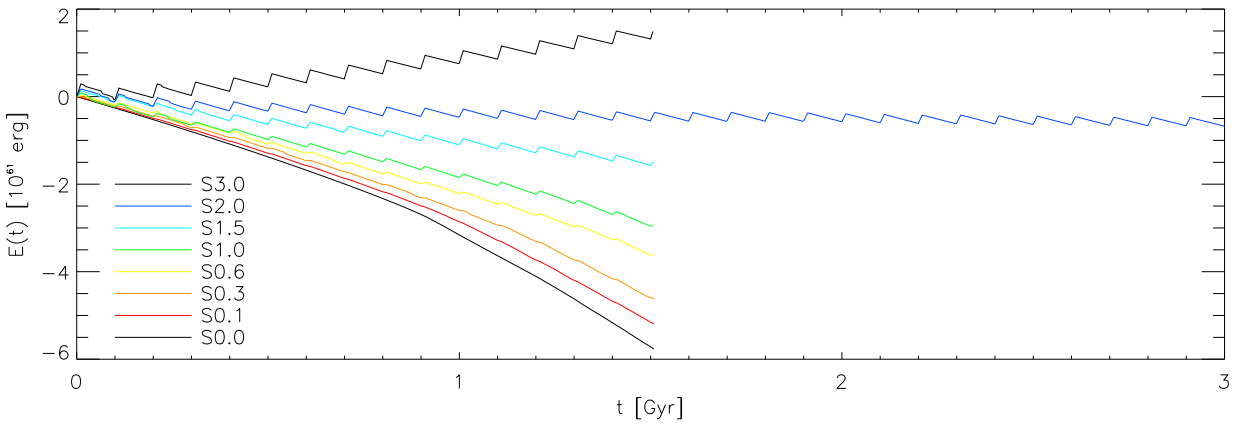

Figure 1. The evolution of the total energy of each simulation is shown by plotting $\Delta E(t) = E_{\rm T}(t) - E_{\rm T}(0)$, where $E_{\rm T}(t)$ is the sum of internal, kinetic and potential energy at time t and $E_T(0)$ is its initial value. The saw-tooth shape of the curves results from the discrete AGN events and subsequent cooling. At the mean injection rate of simulation S2.0, the energy keeps an almost constant value within the simulation time. We tested that this behaviour is maintained up to 5 Gyr, though we show the evolution only to 3 Gyr for clarity.

does not affect the boundaries. This guarantees the hydrostatic equilibrium condition is not broken, and no evident inflow or outflow occurs at the border of the grid. Moreover, the temperature difference between the last computational cell and the guard cell next to it, at the end of the simulation, is always less that 2%. Likewise, sound waves propagating across the volume do not generate any unphysical artifacts at the boundary.

The time step is derived by the Courant condition $\mathrm{d}t = C\Delta x/c_s$, where Δx is the dimension of a cell, c_s is the sound speed in that cell and C is a coefficient, usually less than one. The time step is uniform; thus, all the cells evolve at each time step.

2.2 Initial Conditions

The time-independent gravitational potential of the dark matter is that corresponding to a Navarro, Frenk, & White (1996, 1997) density profile

$$\rho_{\rm DM}/\rho_{\rm crit} = \frac{\delta_{\rm c}}{(r/r_{\rm s})(1+r/r_{\rm s})^2},$$

where $\rho_{\rm crit}$ is the critical density, $r_{\rm s} = r_{200}/c$ and $r_{200} = 1.38$ Mpc. We adopted a halo mass of $M_{200} = 3 \times 10^{14}$ $\mathrm{M}_{\odot}$ and set the concentration parameter to $c = 6$ (Eke, Navarro, & Steinmetz 2001; Wechsler et al. 2002; Dolag et al. 2004).

We use the prescription of Wu, Fabian, & Nulsen (2000) to set up an isothermal gas distribution in hydrostatic equilibrium within this dark matter potential. We adopted this prescription because of its simplicity. Fits to numerical simulations (Komatsu & Seljak 2001), suggest that the temperature should decline with increasing radius. However, our isothermal profiles do match the observed temperature structure of clusters within $0.2r_{200}$, where the observational data show an isothermal temperature profile (eg. Allen, Schmidt, & Fabian 2001; De Grandi & Molendi 2001; Pointecouteau et al. 2004) sometimes with a central decrement. A central decrement is quickly generated as the model cluster cools.

We choose an initial gas temperature of $T = 3.1$ keV, consistent with the observed correlation between temperature and M_{200} (Reiprich & Böhringer 2002). The appropriate gas density is then

$$\rho_{\rm GAS}/\rho_0 = (1 + r/r_{\rm s})^{\eta/(r/r_{\rm s})},$$

where ρ_0 was chosen to satisfy the relation

$$M^{200}_{\rm GAS}/M^{200}_{\rm DM} = \Omega_b/(\Omega - \Omega_b),$$

Here, $M^{200}_{\rm DM}$ denotes dark matter mass contained within a sphere whose mean interior mass density is 200 times the critical density. We used $\eta = 10.25$, $\Omega = 0.3$ and $\Omega_b = 0.04$ for the matter and baryon densities in units of $\rho_{\rm crit}$, and $h = 0.7$ for the Hubble parameter.

We adopt the cooling functions of Theuns et al. (2002), which include cooling by H, He and metals, in the presence of an ionising UV-background. This cooling function uses interpolation tables for the cooling rate due to a solar admixture of metals, obtained from Cloudy (version 94, Ferland et al. 1998). We assume a metallicity of one third solar, and the Haardt & Madau (1996) UV-background at redshift $z = 0$, as updated by Haardt & Madau (2001). The cooling routine was tested against the MEKAL (Mewe, Lemen, & van den Oord 1986) cooling routines in the X-ray analysis package XSPEC (Kaastra 1992) and against the cooling rates used by McCarthy et al. (2004).

Heating by an AGN is modelled by injecting energy at predefined points in space and time. This allows us to simulate multiple episodes of AGN activity as we now describe.

2.3 Energy Injection

To simulate the effect of a central AGN, bubbles of energy are distributed randomly inside a radius of 50 kpc from the centre. We do not attempt to model the processes leading to the formation of the bubbles, but we consider it likely that the bubbles will be injected at different positions because of the precessional motion of the jet axis of the central source.

Energy is injected with a three-dimensional Gaussian

distribution proportional to $e^{(x^2+y^2+z^2)/2\sigma^2}$ and we take the initial size of the bubble to be characterised by $\sigma = 10.3$ kpc. The bubble is truncated at a maximum radius of $r_{\rm b} = 5\sigma = 51.5$ kpc, which is seven cells in our standard six level resolution runs. The final radius (after the expansion of the bubble) depends on the amount of energy injected.

Starting from $t = 0$, energy is injected every 10^8 yr for a time of 10^7 yr in our standard simulations. We assume energy values from 1×10^{59} to 3×10^{60} erg (Table 1). Our choice of parameters deliberately lies at the upper end of observed AGN duty cycles and jet powers (Willott et al. 1999; Owen, Eilek, & Kassim 2000; Fabian et al. 2003; Eilek 2003).

2.4 The Simulations

Our main results are derived from a series of nine simulations (Table 1):

1. an adiabatic test simulation (A) without cooling or AGN bubbles;
2. a simulation with cooling but no AGN bubbles (S0.0);
3. seven simulations with cooling and AGN bubbles of varying strength (S0.1–S3.0), but the same duty cycle. In these simulations only the energy of each bubble varies. The position and timing of the heating events are the same.

The results of these simulations are presented in Section 3.

We also performed simulations with the following changes in order to test the sensitivity of our results to the details of the heating cycle:

4. the bubbles were randomly distributed inside a sphere of 25 or 100 kpc, instead of 50 kpc;
5. the same total number of bubbles (15) was generated within 1.5 Gyr, but at random time intervals;
6. the energy was injected as bubble pairs, with each bubble containing half the energy per event.

Finally, we also reran simulation S2.0 with increased resolution to check for numerical convergence. The results of this test, described in Appendix A, led us to adopt a maximum refinement level of six. We also continued the simulation S2.0 to 5 Gyr to test the long term stability of this simulated cluster.

In the adiabatic simulation, the gas remains almost static as expected for our equilibrium set-up, apart from small re-adjustments induced by discretisation. Energy and mass are conserved to $\simeq 0.4\%$ and 1% respectively. With cooling allowed (simulation S0.0), the loss of pressure support causes a cooling flow to be established.

The intial conditions have a relatively high X-ray luminosity ($\log L_{X,bol} = 45.0$) compared to the observed X-ray luminosities of clusters of this mass and temperature (Markevitch 1998; McCarthy et al. 2004). This is a well-known problem that results from the low entropy gas in the centre of a cuspy dark matter potential. Starting with such a luminous cluster ensures that our simulations conservatively explore the maximum energy necessary to stabilise cooling. In order to be fully successful, however, our energy injection must not only balance the cooling, but also raise the entropy of the cluster gas sufficiently to reduce the total luminosity by a factor ~ 10.

By default, we ran each simulation for 1.5 Gyr. Without a cosmological context, a longer simulation is not well justified since cluster-cluster mergers provide an important additional mechanism for re-organising the gas distribution and erasing the cooling flow structure. Nevertheless, we ran the S2.0 simulation for 5 Gyr to check the evolution of the solution over very long time scales.

3 RESULTS

3.1 The Effect of Energy Injection

In Figure 1 we show, for each simulation, the variation in the total energy within the simulation volume. The pulsed injection of the energy and subsequent cooling gives rise to a saw-tooth pattern.

In simulation S0.0, which has no heating, the cooling rate increases with time as the cluster collapses. Including energy injection (simulations S0.1–S3.0) reduces the overall amount of energy that is radiated. This is not a trivial result since the energy injection events can actually promote cooling in the compressed regions around the rising bubbles. In practice, however, the dominant effect is the mixing of high and low entropy material in the large-scale gas motions induced by the bubbles. Therefore, as the injected energy is increased, the amount of radiated energy drops. At a mean energy injection rate of 6.3×10^{44} erg s^{-1} (simulation S2.0), the radiated energy and the injected energy are balanced. This balance does not guarantee that the structure of the cluster is stable, as continuing collapse of the central region might be balanced by expansion of the outer part of the cluster. However, as Figure 2 shows, the whole entropy profile of the cluster changes little. We investigated the long term behaviour of this model by continuing this simulation for 5 Gyr (Figure 1) and found that the cluster maintains this behaviour even over this longer timescale. Of course, over such long timescales, the effects of cluster mergers can not be neglected.

The emissivity-weighted temperature and entropy profiles of each simulation are shown, for 50 output times, in Figure 2. We define the entropy as $K \equiv kT_e n_e^{-2/3}$ [keV cm^2], where T_e and n_e are the electron temperature and density, respectively. This is related to the thermodynamic entropy by a logarithm and additive constant. If cooling is not balanced by the energy injection, the entropy profile drops dramatically in the centre (top-right plot). This is reflected as a marked dip in the temperature profile of the cluster (top-left plot). Energy injection reduces this trend, maintaining the relatively flat entropy profile and isothermal temperature of the initial cluster.

The cooling of material in the central cluster regions leads to a net inflow of gas. In Figure 3, we plot the mass accumulation rate within the central regions of our simulated clusters. The rate is determined by averaging over the last 0.3 Gyr of the simulation, and is computed within the central 100 kpc and 50 kpc. The results for both radii are similar, as expected if the cluster is in a quasi-steady state. The figure also shows the mass accumulation rate of material with temperatures less than 1 keV. In the absence of energy injection, the cooling cluster deposits material in the cluster centre at a rate that exceeds 1000 M$_\odot$yr^{-1}, a factor $\sim$ 10–100 higher

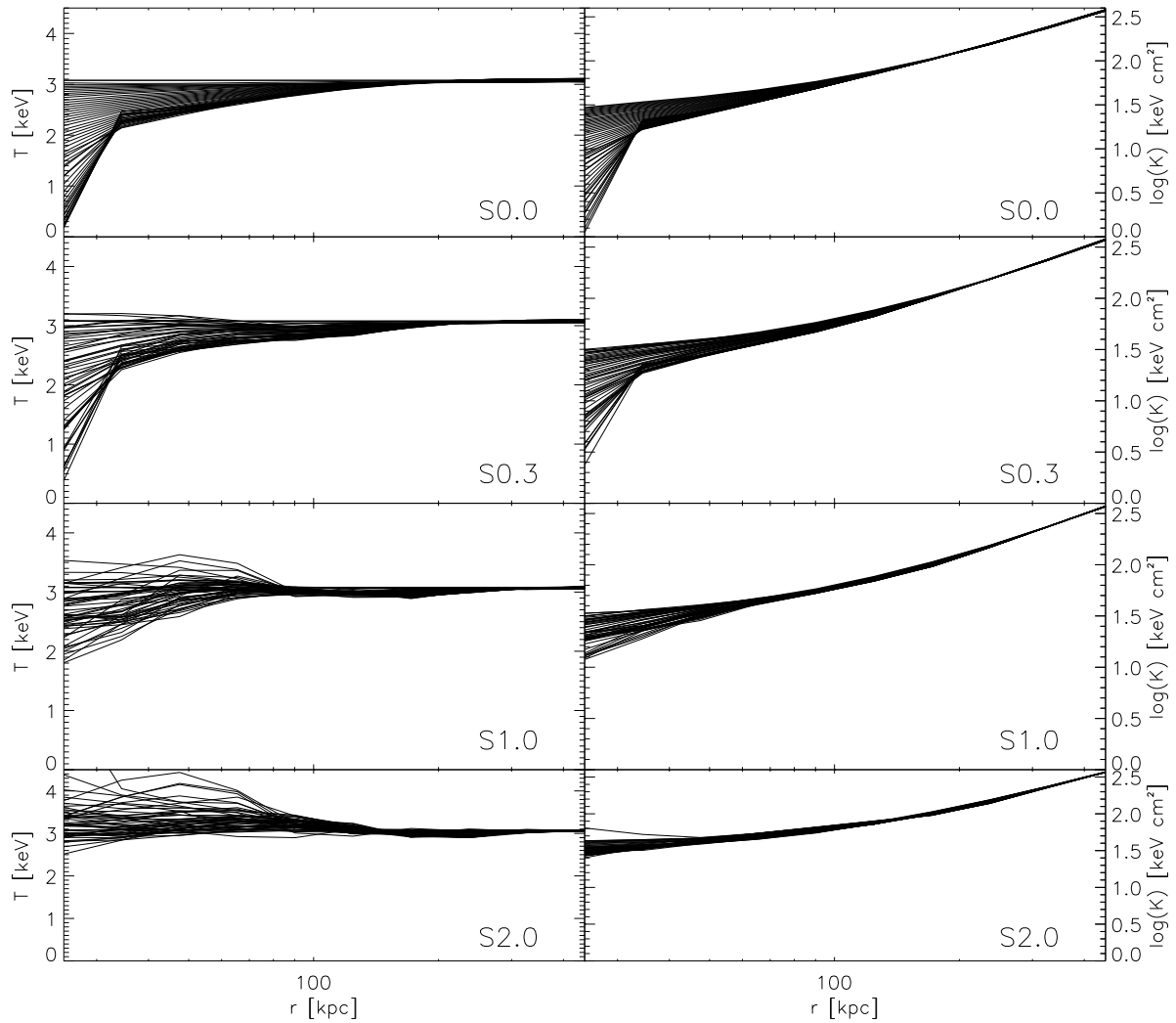

Figure 2. The emissivity–weighted temperature (left panels) and entropy (right panels) profiles of each simulated cluster are shown for 50 simulation times. From top to bottom, simulations S0.0 (without any AGN bubble), S0.3, S1.0 and S2.0 are shown. The effect of energy injection is to maintain the initial, relatively shallow entropy profile and isothermal temperature in the cluster core.

than the observational limits (Crawford et al. 1999; Edge 2001; Salomé & Combes 2003). Similarly, this model has a large mass flux of material cooling below 1 keV (1/3 of the ambient temperature).

Energy input at an average rate of 4.7×10^{44} erg s^{-1} (S1.5) reduces the deposition rate below 30 $M_{\odot}yr^{-1}$ at the end of the simulation, as required by observations (Peterson et al. 2001; Tamura et al. 2001; Kaastra et al. 2001; Peterson et al. 2003). Even with a lower energy injection rate of 3.2×10^{44} erg s^{-1} (S1.0), the rate at which material cools below 1 keV is still consistent with observed X-ray spectra. We conclude that energy injection through the creation of buoyant bubbles can successfully prevent catastrophic cooling.

3.2 Two-dimensional morphologies

In Figure 4, we show the time evolution of various quantities in two-dimensional sections of simulation S2.0. The temperature and entropy distributions are shown for a slice in the x-y plane. They show that cold, low entropy gas is pushed to large radii by the bubble's buoyancy and mixed with gas at those radii. Thus, the cooling rate is reduced not by direct heating of the cooling gas, but by convective transport of this material to regions of lower pressure. Similar results have been seen in simulations of single bubbles (e.g. Quilis, Bower, & Balogh 2001; Churazov et al. 2002).

The temperature distribution also reveals the presence of sound waves propagating through the ICM. The sound waves are almost concentric and regular, a consequence of the periodic energy injection events near the cluster centre.

In order to illustrate what might be observable with an idealised X-ray satellite, we also calculated the projection of the quantity $\rho^2 T^{1/2}$, which is approximately proportional to the bolometric gas emissivity. Despite the large amounts of energy being dumped into the central regions, the large-scale gas distribution appears smooth and undisturbed in projection. To reveal the presence of perturbations

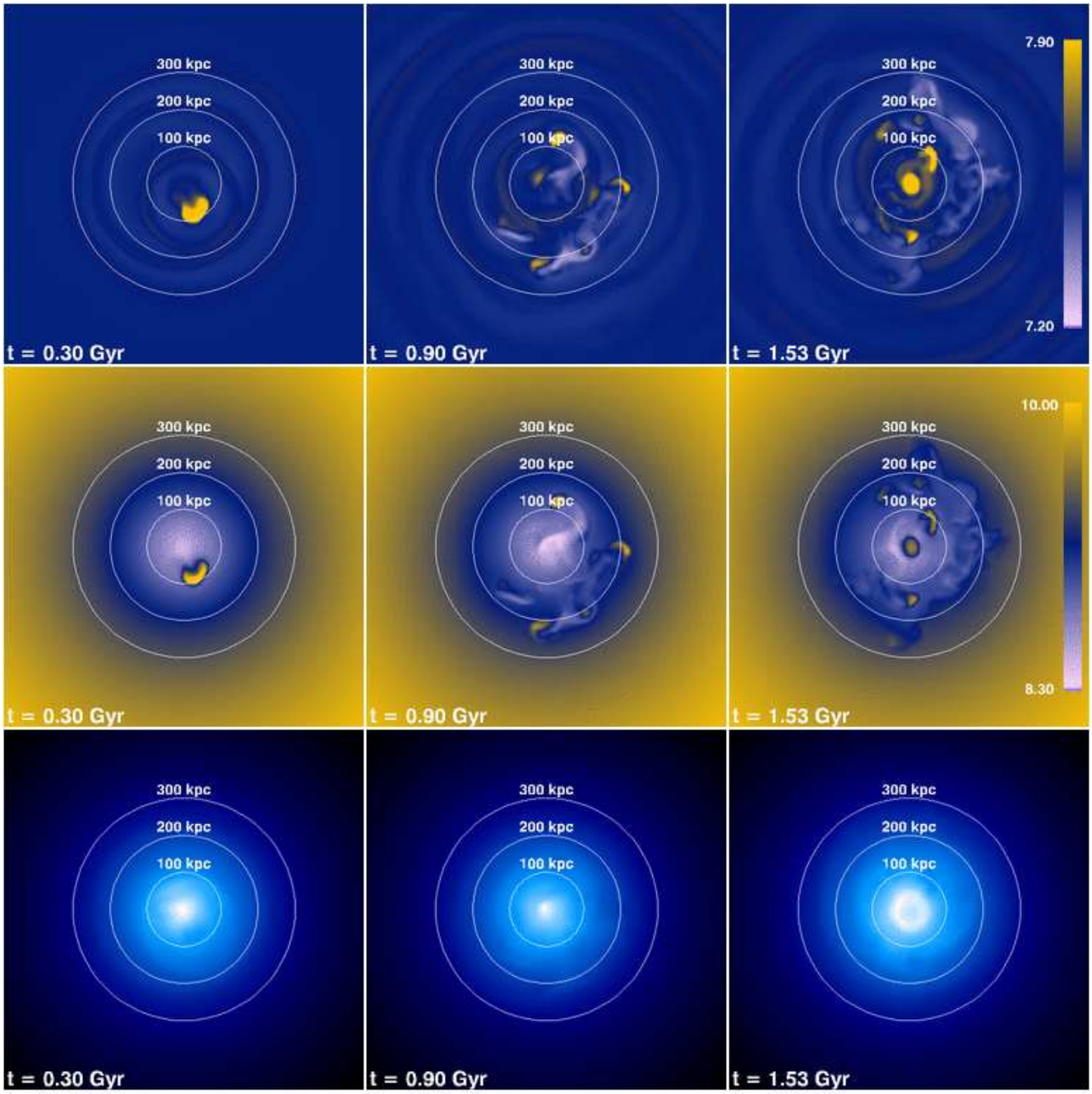

Figure 4. The time evolution (from left to right) of simulation S2.0. From top to bottom, the quantities shown are the temperature [K] and entropy [ergs $g^{-2/3}$ cm^2] on the x-y plane crossing the centre. In the bottom row we show the approximate bolometric emissivity $\rho^2 T^{1/2}$ projected through the simulation volume. The temperature distribution reveals the presence of sound waves propagating through the ICM. The sound waves are almost concentric and regular, a consequence of the periodic energy injection events near the cluster centre.

on this smooth profile, we created an unsharp masked image through the transformation $(\mathrm{img}_0 - \mathrm{img}_s)/\mathrm{img}_s$, where img_0 and img_s are the original image and its smoothed version, respectively. The initial image was taken from a high resolution simulation (~ 2 kpc) and the final unsharped image is shown in Figure 5. The contrast in this image is high enough to show the sound waves distinctly as *ripples*. As suggested by Fabian et al. (2003), these ripples in X-ray images of observed clusters could be the fingerprint of multiple outbursts and could be used to measure their periodicity. Furthermore, if the cluster gas is sufficiently viscous, these sound waves might help to offset the cooling flow by directly heating the gas (Fabian et al. 2003; Ruszkowski, Brüggen, & Begelman 2003). By comparing the properties of successive ripples it may be possible to measure the viscosity of the ICM. Although the ripples in our simulation extend to very large radii, a result of the small viscosity in the simulations, it is unlikely that realistic observations would have sufficient

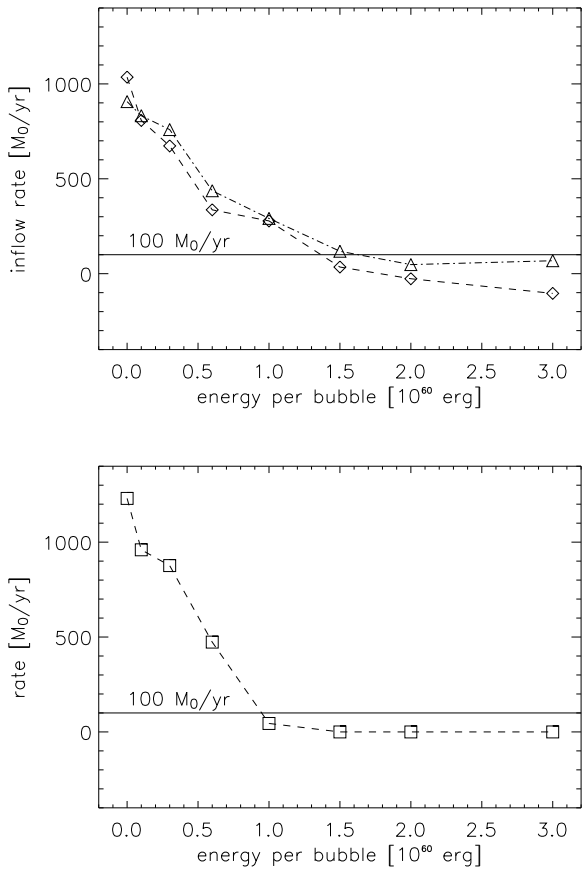

Figure 3. Top panel: The mass deposition rate into a sphere of radius 50 kpc (dashed line) and 100 kpc (dash dotted line), averaged over the time interval 1.2 to 1.5 Gyr, as a function of the energy injected per bubble. For bubbles of energy above 10^{60} erg the deposition rate is $\lesssim 100$ $M_\odot yr^{-1}$. **Bottom panel**: The mean growth rate of the total mass at temperature < 1 keV for each simulation. The amount of gas cooling below 1 keV drops down to almost zero when the injected energy per bubble is greater than 10^{60} erg.

signal–to–noise ratios to see these weak features at such distances. We will investigate this further in a future paper, where we synthesise artificial X-ray images, with the appropriate transmission functions, from our simulations.

3.3 Sensitivity to duty cycle parameters

Simulations S0.1–S3.0 were based on a regular injection of energy. This is somewhat artificial, so we investigated whether randomly–timed energy injection events would have the same effect. We also investigated what happens if the energy injection occurs in less frequent bursts of greater intensity, or if bubbles are distributed inside a sphere of larger (100 kpc instead of 50 kpc) or smaller (25 kpc) radius. All our tests were performed choosing the parameters of simulation S2.0.

The resulting energy evolution of each simulation is illustrated in Figure 6. First, we double the time between bursts, while keeping the total average energy rate constant; thus, each bubble has twice as much energy injection as in S2.0. In this case, the variation in total energy during each cycle is much larger than before. However, the long term evolution is very similar. Randomising the injection time does not have a large effect on the average energy evolution over the duration of the simulation either. Where a particularly long time interval elapses between bubbles, the energy drops further as cooling progresses; however this is offset by later events where bubbles appear in quick succession. Our results are also insensitive to whether the bubbles are injected singly, or in pairs with the total energy divided between the two bubbles, possibly a better model for the AGN activity. The main factor that does make a significant difference is the location of the bubbles. Placing the bubbles initially within a larger radius (100 kpc) is much less effective at disrupting the cooling flow, since these bubbles tend to rise buoyantly without disturbing the central, cooling gas. By the end of this simulation, the total cluster energy has dropped below that of simulation S1.5 and is falling rapidly. Conversely, placing all the bubbles within 25 kpc is much more effective at preventing cooling, and the total energy of the system actually increases with time. To summarise, we see that the energy balance is most sensitive to the total amount of injected energy, and to the initial location of the bubbles.

4 DISCUSSION

4.1 Energy Requirements

Most central galaxies in clusters are radio sources (Ledlow & Owen 1996); we can therefore expect that events like those we have simulated will play an important role in cluster evolution. We have shown that the cluster cooling rate can be reduced so that it agrees with observations if the AGN activity is sufficiently energetic. We have modelled the energy injection events as short outbursts separated by relatively long quiescent periods in order to make an extreme test of the long term effect of the energy injection mechanism. To stabilise the long term evolution of the model cluster in this way, we require an energy of $\sim 2 \times 10^{60}$ erg for each of the injection events, if the bubbles are distributed within a $\sim$ 50 kpc radius. We can associate these events with outbursts of powerful AGN activity with a duration of $\sim 10^7$ yr and a power of $\sim 6 \times 10^{45}$ erg s^{-1}.

The observed radio power of central galaxies varies by factors of ~ 100 for clusters with similar core X-ray luminosities. The most powerful radio sources can have monochromatic radio power of $\nu \cdot S_\nu \sim 10^{41.5}$ erg s^{-1} (where S_ν is the radio luminosity density at $\nu = 1.4$ GHz); around 10% of clusters host such powerful sources. Eilek's (2003) analysis of central cluster radio source morphologies and ages suggests that the ratio of the total jet power ($P_{\rm jet}$) to $\nu \cdot S_\nu$ is more than 10^4. Under minimal assumptions, this can be confirmed in the case of M87, where the most detailed radio observations are available (Owen, Eilek, & Kassim 2000); such powerful jets are also inferred for classical FR II sources (Willott et al. 1999). This power is close to the Eddington limit for accretion by a 10^9 $M_\odot$ black hole. Thus, the total jet power of the most powerful radio galaxies is comparable to the energy required to counter-balance cooling in our simulated cluster. The frequency with which these sources

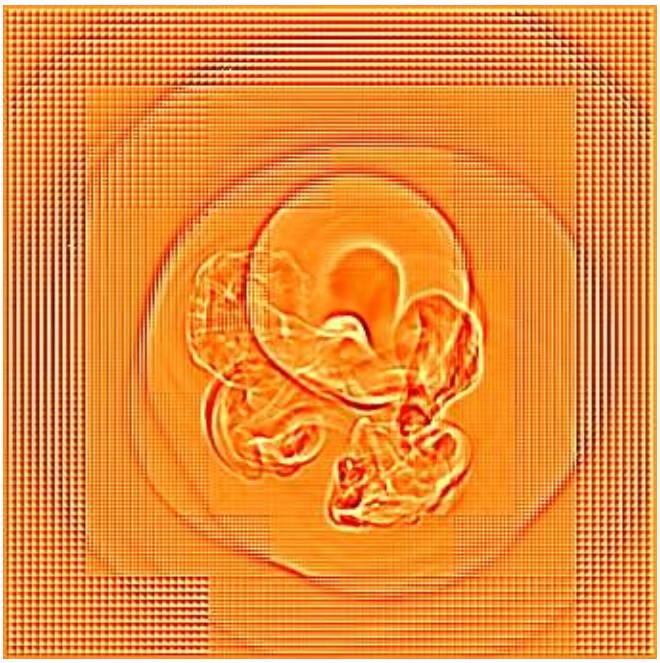

Figure 5. An unsharp masked projection of the approximated X-ray emissivity, $\rho^2 T^{1/2}$, for the central (0.9 Mpc diameter) part of the cluster simulated at a maximum resolution of $\sim$ 2 kpc. The "granular" structure of the image is due to the resolution of the simulation grid. The ripples from successive energy injection events can be clearly seen.

occur in clusters also seems consistent with the duty cycle that we have assumed in our simulations.

It is worthwhile to emphasise that the energy injection can vary significantly (by a $\sim 50\%$) while still reducing the mass deposition rate to an acceptable level after 1.5 Gyr. These variations in the injected energy lead to an overall cooling or heating of the cluster: however subsequent mergers with massive substructures will disrupt the evolution presented in our simulations (which assume a static gravitational potential). The shocks and turbulence generated in the mergers will lead to a re-distribution of energy and entropy that may erase the differences that have built up during the quiescent phase that we simulate (Gomez et al. 2002; Burns et al. 2003). Our model does not contain any mechanism to regulate the energy injection – this would require detailed understanding of the physics powering the central source from the surrounding gas reservoir. However, as Binney & Tabor (1995) (see also Binney 2004) have argued, it seems natural that the cooling rate and the energy injected by the central energy source should be linked. In this case, a balance between heating and cooling is naturally expected when these quantities are integrated over sufficiently long timescales: if insufficient energy is injected into the ICM, the net cooling leads to a high mass deposition rate, and thus an increase in the fueling of the central engine. Nevertheless, the delays inherent in this feedback loop lead to a short-term imbalance, and thus to the out bursts that we model here.

4.2 Global X-ray properties

Although the injected energy is able to counterbalance the cooling flow in the cluster, the effect on the cluster's overall structure is modest, as we showed in Figure 2. In the absence of any heating, cooling causes the central entropy and temperature to drop precipitously. In simulation S1.0, the AGN energy is sufficient to reduce this drop to only $\sim$ 50 per cent. Thus, by preventing runaway cooling, our energy injection mechanism reduces the change in the initial entropy profile of the cluster. The result is that the integrated luminosity and average temperature of the cluster evolve little. Doubling the amount of energy injected (S2.0) results in a small increase in the central temperature ($\sim 30\%$), and a 20% reduction in luminosity.

We simulated an initially isothermal cluster, with temperature observationally consistent with its mass (Reiprich & Böhringer 2002), in order to see how it would evlove in the luminosity-temperature plane. The experiment raises two issues that are not fully resolved by our model: (1) The cluster is too luminous, for its emission weighted temperature, compared with observed clusters (e.g., Markevitch 1998), even when uncorrected for cooling flows (McCarthy et al. 2004). (2) The temperature profiles of the simulated clusters do not show the temperature decrement seen in the central regions of real clusters (e.g. Allen, Schmidt, & Fabian 2001).

In order to lower the luminosity of the simulated cluster enough to agree with observations, we can either adjust the gravitational potential (by assuming a lower halo concentration) or increase the entropy of the central gas. In order to get good agreement with the average luminosities of clusters of this temperature, we would need to adopt $c \sim 3$, well below the concentrations inferred from dark matter simulations (Eke, Navarro, & Steinmetz 2001; Wechsler et al. 2002). On the other hand, the central entropy could be raised to $\gtrsim 160$ keV cm^{-2} (Babul et al. 2002; Voit, Bryan, Balogh, & Bower 2002), which is a factor of five greater than the initial entropy at 20 kpc. Even if enough energy were injected to achieve this (for example by running simulation S2.0 for a much longer time), this would make the core temperature even hotter, exacerbating the disagreement with observed temperature profiles. Thus, we conclude that the initial cluster gas distribution must have been different from the isothermal model we have assumed. Since the high cooling rate of the unperturbed cluster is a direct consequence of its low central entropy (leading to high X-ray luminosity), our energy injection mechanism has removed the symptoms of the overcooling problem, but not addressed its cause.

Global preheating of the intragalactic medium prior to cluster formation should lead to cluster gas distributions with integrated luminosities and temperatures that are consistent with observations (Kaiser 1991; Navarro, Frenk, & White 1995; Ponman, Cannon, & Navarro 1999; Balogh, Babul, & Patton 1999; Muanwong et al. 2002; Borgani et al. 2002). An alternative (but related) possibility is that heating events similar to the ones we have simulated here occur in the cluster progenitors and/or surrounding filamentary structure, at earlier times. Raising the entropy in these lower mass structures may result in

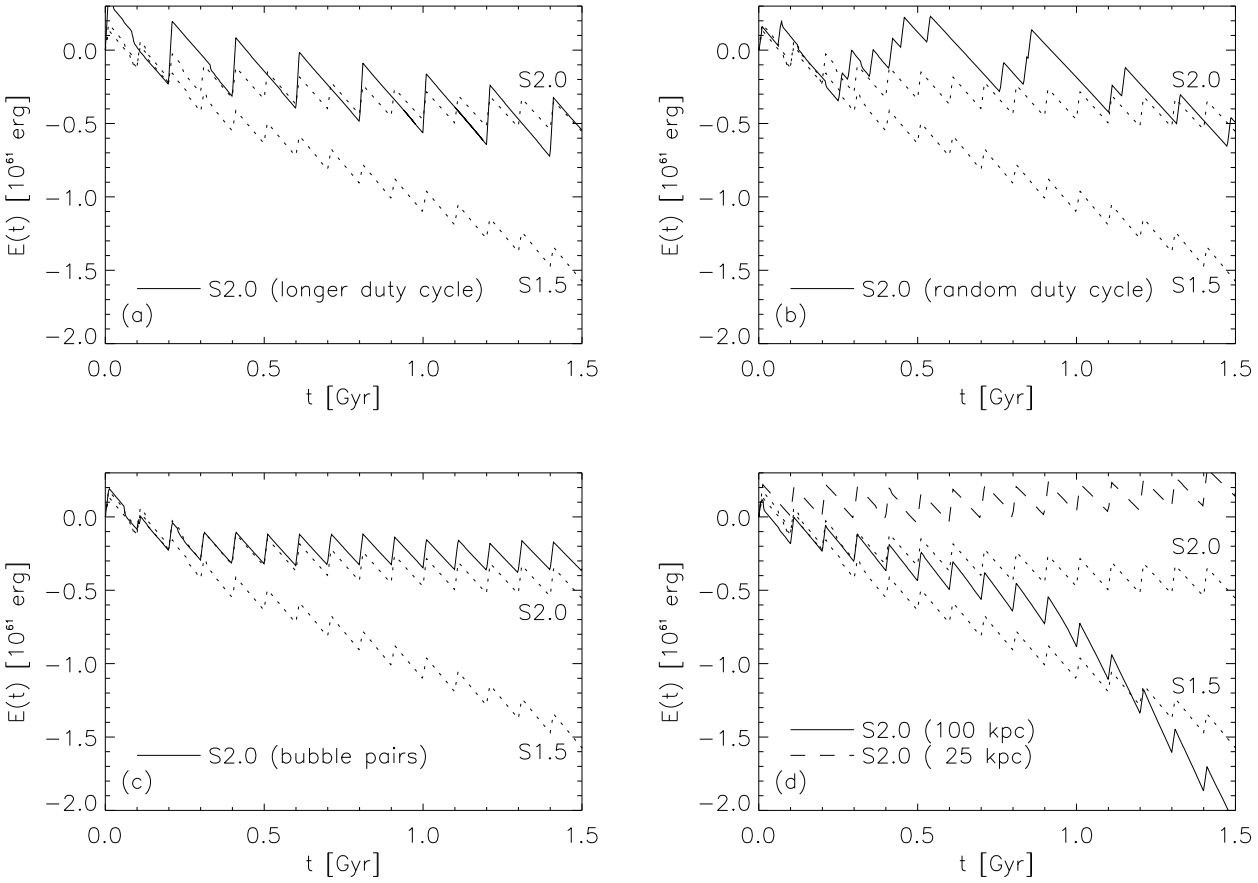

Figure 6. In each panel we show the evolution of the total energy in simulations S2.0 and S1.5 (dotted lines), as in Figure 1. The other lines represent models with the same total energy as simulation S2.0, but with different parameters for the energy injection mechanism. In panel (a) we show a simulation where the duty cycle is regular, but twice as long as in S2.0. In panel (b) we show the effect of randomising the time interval between injection events. In panel (c) we show the effect of injecting the energy within pairs of bubbles. Finally, in panel (d) we show, as the dashed and continuous curves, the effect of placing the bubbles randomly within a 25 kpc or 100 kpc area, respectively.

a higher entropy for the final cluster, as the lower density results in an increase in the accretion shock strength (Voit et al. 2003; Voit & Ponman 2003). In either scenario, subsequent cooling would naturally lead to a temperature decrement in qualitative agreement with observations. Calculations by McCarthy et al. (2004) suggest that although the cluster would then increase in luminosity, it would decrease in emission weighted temperature so as to remain in acceptable agreement with the observed L-T relation.

4.3 Entropy transfer and generation

In Figure 1, we have shown that an energy injection rate of 6.3×10^{44} erg s^{-1} is sufficient for the total energy of the cluster to remain constant and for the density and temperature distribution of the ICM to reach a quasi-equilibrium profile in which the radiative heat losses are balanced by the energy deposited in the ICM by the hot bubbles. The slow evolution of the density profile implies that the energy we inject is somehow shared with the cooling ICM and does not remain trapped in the hot material. In particular, the energy must be efficiently shared with the dense material near the centre of the cluster, where the cooling time is short, leading to an overall increase in entropy in these regions.

There are three mechanisms by which the energy can be shared:

(i) $P\mathrm{d}V$ **work** – as energy is injected into the bubble, it expands doing work on the surrounding material. We calculate the $P\mathrm{d}V$ work by calculating the volume of the bubble at a series of timesteps. 40% of the injected energy is used in this way. The process is largely adiabatic, however, and has little effect on the entropy distribution of the surrounding ICM.

(ii) **shocks** – If the motion of the the bubble were supersonic, shocks would dissipated energy in the surrounding ICM leading to an overall increase in the entropy of the system. In practice, however, the bubble does not reach supersonic speeds: as the speed of the bubble increases the energy dissipation in the turbulent wake grows. In our simulations the maximum Mach number in the flow is 0.8 thus we do not expect shocks to be a major source of entropy in the surrounding ICM.

(iii) **up-lift and turbulence** – The rising bubble generates a complex flow pattern, with material from the central re-

gions of the cluster being up-lifted in the wake behind the bubble. Vortices in this flow dissipate energy and mix the bubble material, low entropy material from the center and the surounding ICM. These irreversible processes generate an increase in the entropy of the cluster.

Even though we assume that the viscosity of the ICM is small, it is certainly not negligible, and viscous dissipation on molecular scales can still be a major source of heating in turbulent regions of the flow. Clearly our simulations are far from resolving the relevant molecular diffusion scales. However, in turbulent flows, the non-linear couplings cause a cascade of energy from large to small scale motions (Kolmogorov 1941). The viscosity determines the smallest scales in the flow, while the rate at which energy is dissipated is determined by the largest scale eddies: these control how quickly energy is fed into the turbulent cascade (Tennekes & Lumley 1972). In simulations, the development of the turbulent cascade is limited by the numerical mixing of fluid elements within a grid cell, rather then molecular viscosity. However, the large scale properties of the flow are not expected to be dependent on the smallest scales that are resolved. We check this by comparing the evolution of a single bubble in two simulations: namely the fiducial resolution and at almost an order of magnitude greater linear resolution. Plotting the two simulations to the same base resolution we see that the gross structure of the flow is the same. Thus, because of the weak dependence of the large scale structure of the flow on the numerical resolution, it is plausible that the energy dissipation and mixing rates in the regions around the rising bubble will converge over the range of resolution that we can test in Appendix A.

In addition to being a source of dissipative energy, the turbulence in the flow provides a means of increasing the entropy of the surrounding ICM through mixing. The mixing may occur between the hot material within the bubble and the surroundings, or between the surrounding ICM and the low entropy material drawn out of the cluster centre by the up-draft created by the rising bubble. In both cases, the mixing is irreversible and leads to an overall increase in the entropy of the system. In the first case, the mixing transfers energy from the bubble to the surrounding ICM (in addition to the $P\mathrm{d}V$ work discussed above). The second case does not directly transfer energy from the bubble, but by driving an entropy increase in the lowest entropy material (the material with the shortest cooling time) it prevents this material cooling out of the flow.

5 CONCLUSIONS

We have presented 3-dimensional gasdynamical simulations using the FLASH adaptive–mesh refinement code of a cooling flow in an isothermal, X-ray luminous cluster of galaxies, with periodic injections of thermal energy. The initial cluster has mass of 3×10^{14} $\mathrm{M}_{\odot}$ and a temperature of 3.1 keV, consistent with the observed mass–temperature relation (Reiprich & Böhringer 2002). The injected energy is manifested as hot bubbles of buoyant gas that rise out of the cluster core, convectively mixing the cooling material. We treat these injection events as sporadic outbursts with a typical duty cycle of 100 Myr. The parameters of these injection events match the observed luminosity and frequency with which the most powerful radio galaxies are seen in clusters.

In the absence of any energy injection, mass rapidly flows to the cluster centre, at a rate that exceeds observational limits by at least an order of magnitude. Based on simulations with a variety of parameters related to the energy injection rate, run for between 1.5 Gyr and 5 Gyr, we draw the following conclusions:

1. For a time averaged energy injection rate of 6×10^{44} erg s^{-1}, the mass inflow rate is less than 30 $\mathrm{M}_{\odot}\mathrm{yr}^{-1}$, compatible with available observational limits. With this amount of heat input, the total energy of the cluster remains approximately constant over 5 Gyr.
2. The evolution of the total cluster energy depends primarily on the total amount of energy injected and the spatial distribution of bubbles, but is only weakly sensitive to the duty cycle of heating events or to whether the bubbles are produced singly or in pairs.
3. The bubble activity generates concentric sound waves that are clearly evident in unsharp–masked projections of cluster emissivity.
4. When the injected energy just balances cooling, the entropy and temperature profile of the cluster remain approximately unchanged from their initial configurations.

In summary, periodic energetic events of the kind we have simulated can reduce the mass flow rate and accumulation of cold gas in massive clusters to within observational limits. However, this mechanism operating on a fully formed cluster does not result in a final luminosity consistent with observations. It is likely that the structure of the progenitors from which the cluster formed was affected by heating events prior to the assembly of the final cluster.

ACKNOWLEDGEMENTS

We thank the anonymous referee for the stimulating questions he posed in his report. We are grateful to Romain Teyssier, Marcus Brüggen and Alastair Edge for helpful discussions. We thank Joop Schaye for allowing us to use his cooling routines. We thank Ian McCarthy for providing his analytic cooling solutions prior to publication, and for his helpful comments on this paper. MLB and RGB acknowledge financial support from PPARC fellowships, PPA/P/S/2001/00298 and PPA/Y/S/2001/00407, respectively. TT thanks PPARC for the award of an Advanced Fellowship. The software used in this work was in part developed by the DOE-supported ASCI/Alliance Center for Astrophysical Thermonuclear Flashes at the University of Chicago.

REFERENCES

Allen S. W., Schmidt R. W., Fabian A. C., 2001, MNRAS, 328, L37
Babul A., Balogh M. L., Lewis G. F., Poole G. B., 2002, MNRAS, 330, 329
Balogh M. L., Babul A., Patton D. R., 1999, MNRAS, 307, 463
Basson J. F., Alexander P., 2003, MNRAS, 339, 353

Binney J., 2004, MNRAS, 347, 1093
Binney J., Tabor G., 1995, MNRAS, 276, 663
Borgani S., Governato F., Wadsley J., Menci N., Tozzi P., Quinn T., Stadel J., Lake G., 2002, MNRAS, 336, 409
Bower R. G., Benson A. J., Lacey C. G., Baugh C. M., Cole S., Frenk C. S., 2001, MNRAS, 325, 497
Brüggen M., Kaiser C. R., 2001, MNRAS, 325, 676
Brüggen M., 2003, ApJ, 592, 839
Burns J. O., Motl P. M., Norman M. L., Bryan G. L., 2003, astro, astro-ph/0309836
Churazov E., Sunyaev R., Forman W., Böhringer H., 2002, MNRAS, 332, 729
Crawford C. S., Allen S. W., Ebeling H., Edge A. C., Fabian A. C., 1999, MNRAS, 306, 857
De Grandi S., Molendi S., 2001, ApJ, 551, 153
Dolag K., Jubelgas M., Springel V., Borgani S., Rasia E., 2004, astro-ph/0401470
Eke V. R., Navarro J. F., Steinmetz M., 2001, ApJ, 554, 114
Edge A. C., 2001, MNRAS, 328, 762
Edge A. C., Wilman R. J., Johnstone R. M., Crawford C. S., Fabian A. C., Allen S. W., 2002, MNRAS, 337, 49
Edge A. C., Frayer D. T., 2003, ApJ, 594, L13
Eilek J. A., 2003, astro, astro-ph/0310011
Fabian A. C., Nulsen P. E. J., 1977, MNRAS, 180, 479
Fabian A. C., Sanders J. S., Allen S. W., Crawford C. S., Iwasawa K., Johnstone R. M., Schmidt R. W., Taylor G. B., 2003, MNRAS, 344, L43
Ferland G. J., Korista K. T., Verner D. A., Ferguson J. W., Kingdon J. B., Verner E. M., 1998, PASP, 110, 761
Fryxell B. et al., 2000, ApJS, 131, 273
Gomez, P. L.; Loken, C.; Roettiger, K.; Burns, J. O., 2002, ApJ, 569, 122
Haardt F., Madau P., 1996, ApJ, 461, 20
Haardt F., Madau P., 2001, cghr.conf
Jaffe, W. & Bremer, M. N. 1997, MNRAS, 284, L1
Johnstone, R. M., Fabian, A. C., & Nulsen, P. E. J. 1987, MNRAS, 224, 75
Kaastra, J. S. 1992, SRON, Leiden report
Kaastra J. S., Ferrigno C., Tamura T., Paerels F. B. S., Peterson J. R., Mittaz J. P. D., 2001, A&A, 365, L99
Kaastra J. S. et al., 2004, A&A, 413, 415
Kaiser N., 1991, ApJ, 383, 104
Kolmogorov, A. N., 1941, C. R. Acad. Sci. URSS, 30, 301
Komatsu, E., Seljak, U., 2001, MNRAS, 327, 1353
Ledlow M. J., Owen F. N., 1996, AJ, 112, 9
Loken C., Norman M. L., Erik N., Burns J., Bryan G. L., Motl P., 2002, ApJ, 579, 571
McCarthy, I. et al., MNRAS, submitted
Markevitch M., 1998, ApJ, 504, 27
Mewe, R., Lemen, J. R., & van den Oord, G. H. J. 1986, A&AS, 65, 511
Motl, P. M., Burns, J. O., Norman, M. L., & Bryan, G. L. 2003, ArXiv Astrophysics e-prints, 9828
Muanwong O., Thomas P. A., Kay S. T., Pearce F. R., 2002, MNRAS, 336, 527
Navarro J. F., Frenk C. S., White S. D. M., 1995, MNRAS, 275, 720
Navarro J. F., Frenk C. S., White S. D. M., 1996, ApJ, 462, 563
Navarro, J. F., Frenk, C. S., & White, S. D. M. 1997, ApJ, 490, 493
O'Connell, R. W. & McNamara, B. R. 1989, AJ, 98, 180
Omma, H., Binney, J., Bryan, G., & Slyz, A. 2003, ArXiv Astrophysics e-prints, 7471
Omma H., Binney J., Bryan G., Slyz A., 2004, MNRAS, 348, 1105
Owen F. N., Eilek J. A., Kassim N. E., 2000, ApJ, 543, 611
Peterson, J. R. et al. 2001, A&Ap, 365, L104
Peterson, J. R., Kahn, S. M., Paerels, F. B. S., Kaastra, J. S., Tamura, T., Bleeker, J. A. M., Ferrigno, C., Jernigan, J. G., 2003, ApJ, 590, 207
Pointecouteau, E., Arnaud, M., Kaastra, J. S., de Plaa, J., 2004, astro-ph/0403596
Ponman T. J., Cannon D. B., Navarro J. F., 1999, Nature, 397, 135
Quilis, V., Bower, R. G., & Balogh, M. L. 2001, MNRAS, 328, 1091
Reiprich T. H., Böhringer H., 2002, ApJ, 567, 716
Reynolds, C. S., Heinz, S., & Begelman, M. C. 2002, MNRAS, 332, 271
Reynolds C. S., McKernan B., Fabian A. C., Stone J. M., Vernaleo J. C., 2004, astro, astro-ph/0402632
Romanishin, W. 1987, ApJl, 323, L113
Ruszkowski M., Brüggen M., Begelman M., 2003, astro, astro-ph/0310760
Ruszkowski M., Brüggen M., Begelman M. C., 2004, astro, astro-ph/0403690
Salomé, P. & Combes, F. 2003, A&Ap, 412, 657
Tabor G., Binney J., 1993, MNRAS, 263, 323
Tamura T. et al., 2001, A&A, 365, L87
Tennekes, H. & Lumley, J. L. 1972, A First Course in Turbulence, The MIT Press
Theuns, T., Schaye, J., Zaroubi, S., Kim, T., Tzanavaris, P., & Carswell, B. 2002, ApJL, 567, L103
Voigt, L. M. & Fabian, A. C. 2003, ArXiv Astrophysics e-prints, 8352
Voit, G. M., Bryan, G. L., Balogh, M. L., & Bower, R. G. 2002, ApJ, 576, 601
Voit G. M., Balogh M. L., Bower R. G., Lacey C. G., Bryan G. L., 2003, ApJ, 593, 272
Voit G. M., Ponman T. J., 2003, ApJ, 594, L75
Wechsler R. H., Bullock J. S., Primack J. R., Kravtsov A. V., Dekel A., 2002, ApJ, 568, 52
Willott C. J., Rawlings S., Blundell K. M., Lacy M., 1999, MNRAS, 309, 1017
Woodward & Colella (Woodward P., Colella P., 1984, JCP, 54, 115
Wu, K. K. S., Fabian, A. C., & Nulsen, P. E. J. 2000, MNRAS, 318, 889

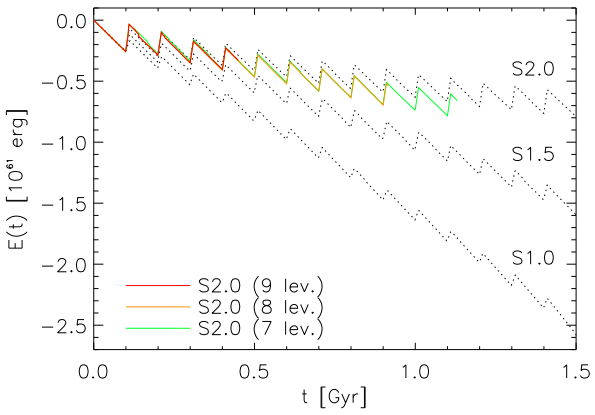

Figure A1. As Fig. 1, the energy evolution is shown for the simulations S1.0, S1.5 and S2.0 run with 6 levels of refinment (black, solid lines). We compare these with simulation S2.0 run at different resolutions (7, 8 and 9 refinement levels).

APPENDIX A: RESOLUTION CONVERGENCE TESTS

We tested the convergence of the code by running simulation S2.0 at increased resolution. In Figure A1 we compare the total energy evolution for simulation S1.0 (6 levels of refinement, resolution of 7.6 kpc) and S2.0 (6, 7 (3.8 kpc), 8 (1.9 kpc) and 9 (0.9 kpc) levels of refinement). The codes were run for different lengths of time because of the limitation of the computational time and memory available. The differences between the four versions of the S2.0 run are small in comparison to the relative evolution of the S1.5 and S2.0 simulations. The figure also shows that the radiated energy does not increase systematically with resolution. Comparing the total radiated energy at $t = 0.45$ Gyr, the four versions of the S2.0 simulation differ by less than 3%. At the last common output time, the 6 and 7 level simulations differ by 4%. We also compared the density and entropy profiles of the simulations at this output time, and found a similar level of agreement. We therefore chose to run the code with a maximum refinement level of 6, this being a good compromise between the speed of the code and the desired accuracy of the relevant quantities.

Simulation S0.0 was also used to check the convergence of energy conservation as the maximum number of levels of refinement changes. With just 4 refinement levels, the total energy has an error of $\sim 1\%$, while with 6 levels the error is less than 0.1%. We decided to run the simulations with a maximum number of 6 levels. The equivalent resolution of a fixed-grid Eulerian code is 256^3.